The Adsorption of Lemon Yellow Dye Using Cationic Cellulose Fibers from Rice Straw as a Sustainable Biosorbent in Aqueous Media

Zhixin Gu,[a,b] Sijia Zhang,[a] Chuanqing Zhu,[b] and Lijuan Wang [a,*]

A biosorbent was prepared from the cellulose fibers found in rice straw through cationic modification. The effects of the dosage, pH, contact time, and initial concentration of lemon yellow dye were explored. The static adsorption results showed that cationic modification drastically improved the adsorption capacity of straw cellulose fiber. The maximum equilibrium adsorption capacity value was 137.6 mg/g and the highest removal reached 99%. The pseudo-second-order kinetic model was a good fit for the adsorption process, together with the Langmuir isotherm model. The adsorption reaction was spontaneous, and the adsorption process was an exothermic reaction, which was shown by the thermodynamic model. As the adsorption time became longer, the effluent concentration became larger until reaching equilibrium. The time was 420 min. After desorption using a dilute NaOH solution, the maximum adsorption capacity was still 36.1 mg/g and the maximum removal still reached 36.2%. The parameters calculated from the Yoon-Nelson model have a good fit with the experimental data. In short, cationic straw cellulose fiber is an effective and easy to prepare biosorbent. This work offers a new method for dye wastewater purification and solves the effective utilization of rice straw resources.

Keywords: Rice straw; Cationic; Cellulose fiber; Lemon yellow dye; Adsorption

Contact information: a: Key Laboratory of Bio-based Materials Science and Technology of Ministry of Education, Northeast Forestry University, Harbin 150040 PR China; b: College of Information and Computer Engineering, Northeast Forestry University, Harbin 150040 PR China;
** Corresponding author: donglinwlj@163.com*

INTRODUCTION

Dye is widely used in many fields, but it easily pollutes the environment (Baldikova *et al*. 2015). The characteristics of dye wastewater has a complex composition, deep color, high toxicity, strong acidity, and high COD content, and has always been a problem in terms of environmental protection (Heibati *et al*. 2015; Zhang *et al*. 2017).

There are three common treatment methods for dye-polluted water: physical, chemical, and biosorption (Elumalai *et al*. 2016; Asfaram *et al*. 2017). Each method has its own advantages and disadvantages. Electrochemical methods have different decolorization effects on different dyes (De *et al*. 2018). However, they are highly efficient in avoiding secondary pollution (Alver *et al*. 2017). The follow-up treatment is simple, but its cost and energy consumption are high. The advantages of the biological method include high purification efficiency, low price, and no secondary damage to water. However, the decolorization rate and COD removal are not high (Sun *et al*. 2016). The adsorption method is a physical method that is simple to use and yields a strong purification effect, *etc*. However, the adsorbent has a high cost and often cannot be reused (Patil *et al*. 2015).

Moreover, improper subsequent treatment may cause secondary pollution. To date, the adsorption property of activated carbon is widely used to treat dye wastewater. It has a porous structure, high specific surface area, and high absorptivity (Ge *et al.* 2016; Ciftci *et al.* 2018). However, its disadvantages are it is difficult to regenerate, has a high cost, and the possibility of recycling is low (Sudhan *et al.* 2016). However, biosorbents can make up for the disadvantages of activated carbon adsorption.

It is estimated that China produces 300 million tons of rice straw a year (Zhu *et al.* 2017). A primary use of rice straw involves its crushing in the field for the preparation coal-based fuel for heating. However, a large part of it is still directly incinerated, which not only wastes resources but also seriously pollutes the environment (Fan *et al.* 2017; Zazycki *et al.* 2017). The primary components of rice straw are cellulose (43.2%), hemicellulose (11.5%), and lignin (28.9%). Rice straw is rich in hydroxyl groups, aldehyde groups, and carboxyl groups, as well as other active groups, which can undergo a variety of chemical modification reactions (Chen *et al*. 2019). Recently, using rice straw as a biosorbent to adsorb dye wastewater has been a popular research topic.

From this perspective, many studies have made a lot of progress. A solid adsorbent used for SO_2 adsorption was prepared from magnesium salt/rice straw *via* co-precipitation/ calcination (Hosseini *et al.* 2018). Xia *et al.* (2013) used rape straw to extract natural cellulose and prepared several adsorbents for organic dye wastewater treatment with good results. Xie *et al.* (2019) prepared a wheat straw cellulose/GO composite material for the removal of Cd^{2+} and Pb^{2+} from water and the removal reached 93.25%. Halysh *et al.* (2020) determined the adsorption capacity for methylene blue (68.8 mg/g) using a lignocellulosic sorbent derived from sugar cane straw. Fiber biosorbents have a low-cost and abundant; the problem is their low adsorption capacity and as such, it needs modification to improve its adsorption capacity.

Hu *et al.* (2016) used cationic flax noil cellulose as an adsorbent to remove ciprofloxacin from an aqueous solution and confirmed that the cationic groups had been successfully bound to the cellulose molecules after functionalization. Li *et al.* (2019) showed that $KMnO_4$-modified rice husk can be used as an effective alternative adsorbent for the removal of malachite green (MG) from wastewater, with an adsorption rate greater than 90%. Ghasemi *et al.* (2020) used modified barley straw to remove MG from industrial wastewater. The removal efficiency of MG increased as the modified barley straw dosage, pH, and contact time were increased (Ghasemi *et al.* 2020). Hu *et al.* (2019) developed wheat straw modified with maleated rosin to improve its adsorption capacity for methylene blue (MB) dyes, with an adsorption capacity of 113.3 mg/g. Lima *et al.* (2018) studied MG adsorption by raw and modified corn straw (MCS) and the adsorbed quantity at saturation ranged from 164.2 mg/g to 528.2 mg/g.

All the above studies focused on the static adsorption characteristics of modified cellulose adsorbents prepared from straw. These adsorbents had a low adsorption capacity. Very few studies have been done on the application of modified straw cellulose in dye treatment, especially in terms of the dynamic adsorption performance, which can describe the practical application more intuitively and provide data for industrial design. In order to further improve the adsorption capacity, rice straw was modified *via* cationization to prepare cationic straw cellulose fiber (CSCF), which could purify anionic dye solutions. On the basis of studying the static adsorption, this work studied the dynamic adsorption characteristics of lemon yellow (LY) dye using CSCF. It is mainly used for coloring food, beverage, medicine, cosmetics and wool. Lemon yellow wastewater has deep chroma and high COD content, which is one of the difficulties in dye wastewater treatment. The Yoon-

Nelson model was used to simulate the dynamic adsorption behavior to provide basic data for industrial applications. This cheap and efficient biomass material will bring new economic and social benefits to dye wastewater treatment.

EXPERIMENTAL

Materials

Caustic soda SCF was prepared in the laboratory. The sodium hypochlorite (NaClO, 120 g/L) and hydrochloric acid (HCl, 36%) was purchased from Shanghai Shenmei Pharmaceutical Technology Co., Ltd. (Shanghai, China). The sodium hydroxide (NaOH), triethylamine ($C_6H_{15}N$), epichlorohydrin (C_3H_5ClO), anhydrous ethanol (C_2H_5OH), and LY ($C_{16}H_9N_4Na_3O_9S_2$) were analytical reagent grade purchased from Yongda chemical Reagent Co. Ltd (Tianjin, China).

Preparation of the Cationic Straw Cellulose Fiber (CSCF)

In order to be able to remove anionic substances from solution, the SCF was cationized. The NaClO solution was well mixed with SCF and stirred at a temperature of 35 °C for 1 h at a constant temperature *via* a constant speed agitator (JJ-1B). The moisture was filtered out, and the material was rinsed to remove the residual NaClO. The SCF before and after bleaching is shown in Figs. 1a and 1b. The SCF with an 80 mesh to 120 mesh size was selected using an electric vibrating screen (8411), as shown in Fig. 1c. The qualified SCF and NaOH solution (20%) were added to a beaker and stirred *via* a water bath thermostatic oscillator (DSHZ-300A). A triethylamine ethanol solution with a volume fraction of 34% was added into the flask, which was stirred at a temperature of 80 °C for 3 h. The resulting solution was filtered and rinsed to remove the residual triethylamine. Finally, the CSCF was put into a vacuum drying oven (DZ-2AII) at a temperature of 60 °C, as shown in Fig. 1d.

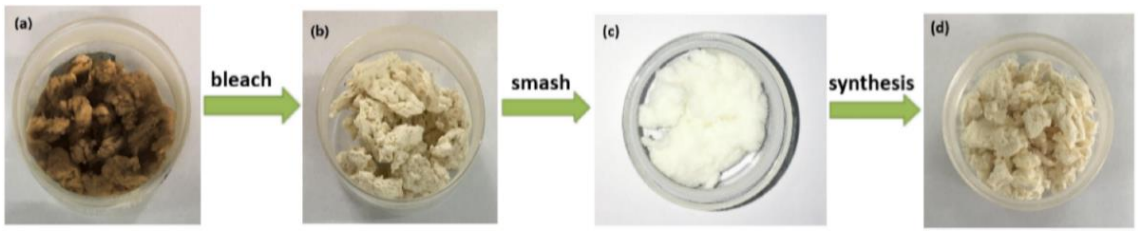

Fig. 1. CSCF preparation process

Characterization of the Cationic Straw Cellulose Fiber (CSCF)

The morphology of samples was examined *via* a Quanta 200 scanning electron microscope (Philips-FEI Co., AMS, Netherlands), with an accelerating voltage of 20 kV. The morphology of the CSCF was observed using a JEM-2100 transmission electron microscope (TEM).

Adsorption Process

The effects of the adsorbent dosage, pH, contact time, and initial concentration of LY dye on the CSCF adsorption were studied. Different amounts of CSCF adsorbent and contact time were demonstrated at various time intervals (10 min to 180 min). The CSCF

adsorbent and LY dye solution were added into a conical flask at various initial LY dye concentrations (20 mg/L, 40 mg/L, 60 mg/L, 80 mg/L, and 100 mg/L). The solution was shaken at temperatures of 30 °C, 40 °C, and 50 °C and at pH values of 2, 4, 6, 8, 10, and 12. After filtration, the absorbance was measured, and the concentration of the residual dye after adsorption (C_e) was calculated from the standard curve. The adsorption capacity (Q) and removal rate (ω) were calculated using Eqs. 1 and 2,

$$Q = \frac{(C_o - C_e) \times V_o}{m} \quad (1)$$

$$\omega = \frac{(C_o - C_e) \times 100\%}{C_o} \quad (2)$$

where m is the mass of the adsorbent (mg), V_o is the volume of solution (mL), and C_o and C_e are the initial and final equilibrium concentrations (mg/L).

Dynamic Adsorption

The CSCF adsorbent (0.9 g) was put into a column (the column diameter was 3.0 cm and the column height was 11.5 cm) as the stationary phase, and the adsorption bed height was 2.0 cm (Fig. 2a). The flow rate of the LY solution (45 mg/L and 50 mg/L) was 5 mL/min, and the effluent solution was collected. The absorbance of the filtrate was measured for each 5 mL solution (Fig. 2b).

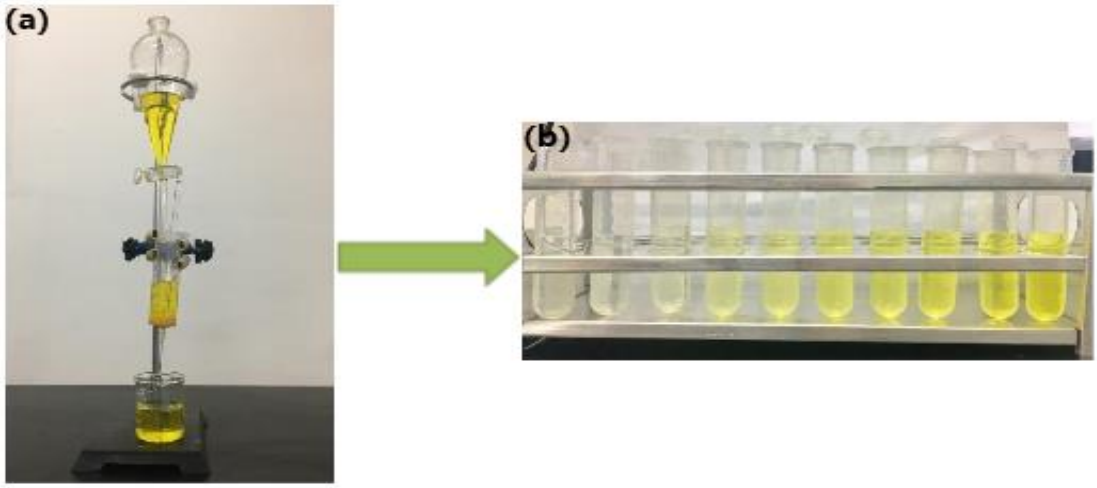

Fig. 2. Dynamic adsorption process

Desorption and Secondary Adsorption

The CSCF after undergoing saturation adsorption (Fig. 3a) and the NaOH solution (0.1 mol/L) were added into conical flasks. Desorption was conducted by shaking at a temperature of 30 °C for 5 min to 50 min. The CSCF after filtering and desorption is shown in Fig. 3b. The absorbance of the filtrates were measured, respectively. The solution concentration after desorption and the desorption rate of the CSCF after saturated adsorption were calculated. The CSCF adsorbent after desorption and the LY dye solution (50 mg/L) were added into the conical flask. After shaking and filtration, the secondary adsorption of LY dye occurred (Fig. 3c) and the C_e, Q, and ω after the desorption occurred were calculated.

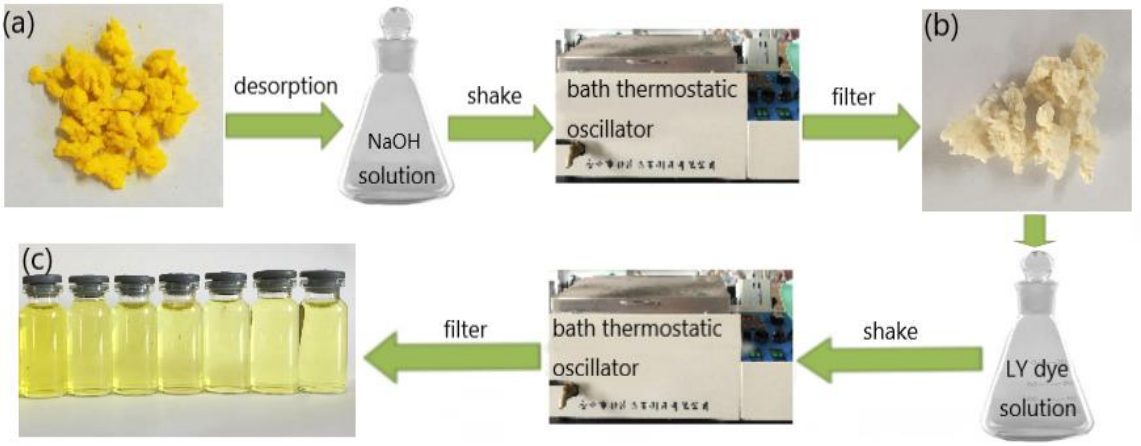

Fig. 3. Desorption and secondary adsorption

RESULTS AND DISCUSSION

Scanning Electron Microscopy (SEM) Analysis

The SEM images of the SCF and CSCF are shown in Figs. 4a and 4b. The surface morphology of the SCF and CSCF had obviously changed. The SCF was filamentous, with many large gullies on the surface and a small amount of impurities. The surface of the CSCF had fewer impurities and was fully saturated. There were some tiny gullies on the surface and some relatively small pore structures of different sizes. These changes visible in the SEM images suggest an increase in surface area, which would be favorable for adsorption interactions.

Fourier-Transform Infrared Spectroscopy (FTIR) and X-Ray Diffraction (XRD) Analysis

The FTIR spectra of the SCF and CSCF are shown in Fig. 4c. The absorption peak of SCF at 3330 cm^{-1} is the vibration absorption peak of O-H. The telescopic vibration peak of C-H in -CH_2- occurs at 2900 cm^{-1}. The telescopic vibration peak of C=O occurs at 1743 cm^{-1}. The lactone and O-H in-plane bending vibration peak occurs at 1316 cm^{-1}. The peak at 1028 cm^{-1} represents the telescopic vibration peak of the cellulose skeleton. The spectrum of CSCF shows that the strength of the telescopic vibration peak of O-H is obviously weakened and deviates towards a high wave number. The strength of the absorption peak of C-H in -CH_2- is slightly enhanced, which showed that the new CH_2^- group was successfully introduced into the SCF molecules. The telescopic vibration peak of C-N is shown at 1470 cm^{-1}, and the CSCF spectra had less miscellaneous peaks than the SCF spectra. These findings demonstrate that the quaternary ammonium group molecular structure was successfully introduced into the molecular structure of SCF, which indicated that the CSCF was indeed synthesized.

As can be seen from Fig. 4d, the characteristic peaks at 15.52° and 22.32° show that SCF was a typical cellulose I-type structure. There was only one characteristic peak at 20.26°. After cationic modification, the intermolecular and intramolecular hydrogen bonds of SCF were destroyed, which resulted in a change of crystal shape.

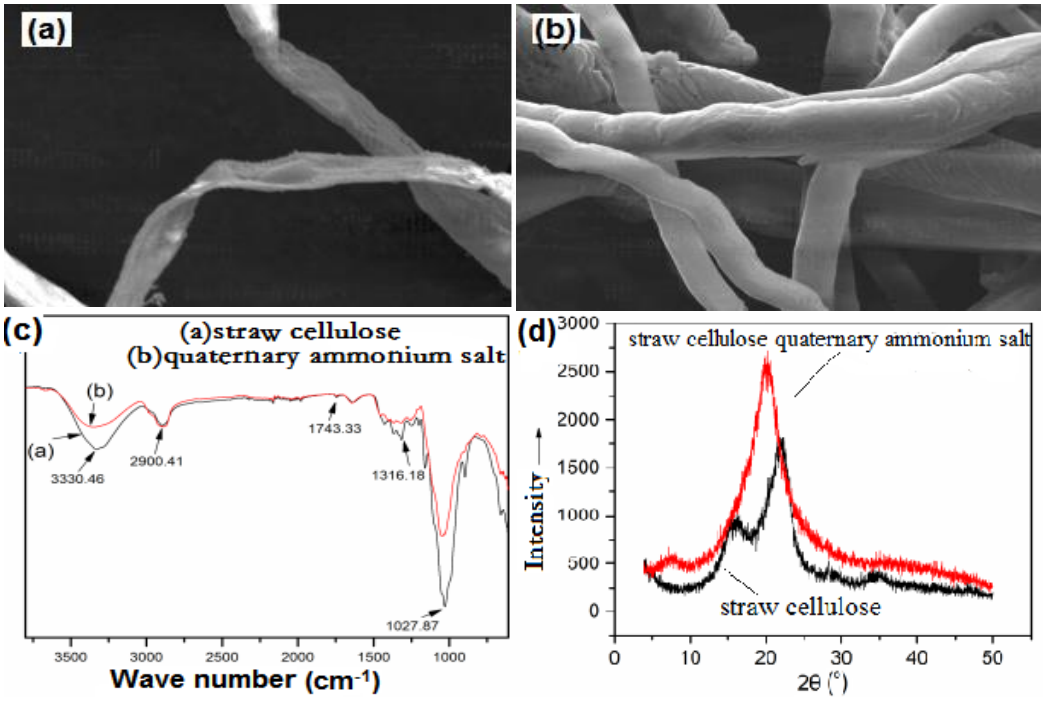

Fig. 4. Characterization images of the SCF and CSCF

Purification Performance

As shown in Figs. 5a and 5b, the adsorption capacity for LY dye was able to reach 138 mg/g, and it gradually decreased as the CSCF dosage was increased. The percentage of removal gradually increased until the system reached equilibrium, with a maximum of 99.3%. The optimal CSCF dosage is 0.05 g.

Rapid adsorption occurred within 30 min, whereas the period of 30 to 90 min was characterized by slow adsorption, as shown in Figs. 5c and 5d. After 90 min, the system reached equilibrium adsorption. The optimal adsorption time was judged to be 90 min, the highest adsorption capacity was 84.0 mg/g, and the maximum removal was 84.3%. As the temperature increased, the adsorption capacity and removal rate decreased at the same contact time, which indicated an exothermic reaction.

The maximum adsorption capacity was 94.0 mg/g, as shown in Figs. 5e and 5f. The optimal initial concentration was judged to be 50 mg/L. The removal percentage was 96.4% at its highest. The increase of the initial concentration not only increases the probability of collision between dye molecules and the adsorbent, but it also increases the concentration difference between the surface of the adsorbent and the main body of the solution.

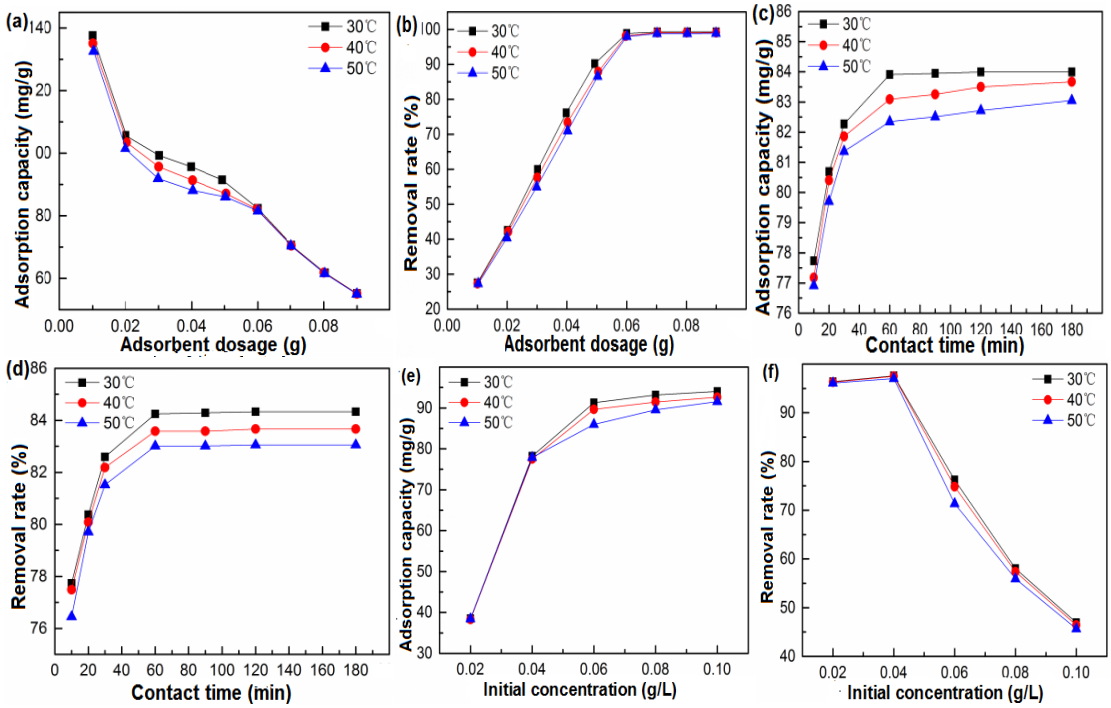

Fig. 5. Purification performance

As shown in Fig. 6, the pH had a strong influence on the adsorption of LY dye solution by CSCF. When the LY dye has an optimal pH of 4, the adsorption capacity and removal rate can reach 88.7 mg/g and 88.7%, respectively.

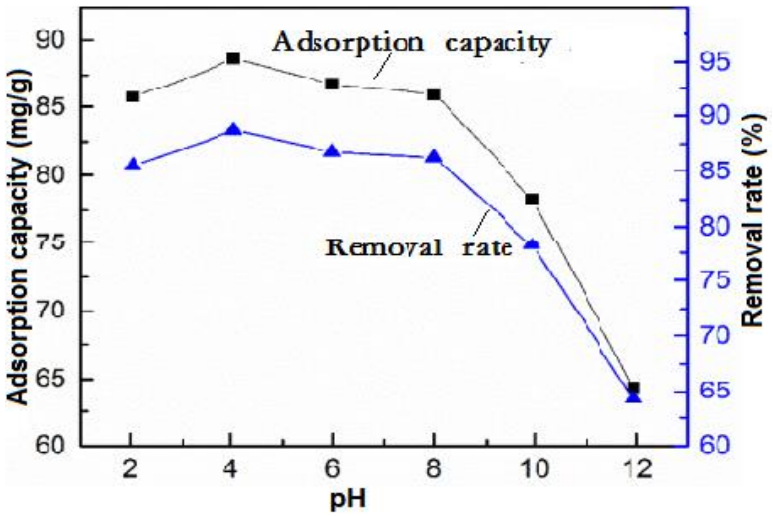

Fig. 6. Effects of different pH values on the purification performance

Adsorption Kinetics

Adsorption kinetics studies the relationship between the adsorption capacity and the contact time, *i.e.*, the adsorption rate and the dynamic equilibrium of adsorption.

Pseudo-first-order kinetic model

Assuming that the adsorption is mainly affected by diffusion, it can be calculated according to Eq. 3,

$$\ln(q_e - q_t) = ln\, q_e - k_1 \quad (3)$$

where k_1 is the rate constant (min^{-1}), q_e and q_t are the adsorption capacity at equilibrium and at time t (mg/g). The conclusion is that the adsorption rate is proportional to q_e minus q_t.

According to the experiment data, the relationship between $\ln(q_e\text{-}q_t)$ and t at different times is shown in Fig. 7a. The constants and adsorption capacity were calculated using the slope and intercept of the line.

Pseudo-second-order kinetic model

The expression of the pseudo-second-order kinetic model is shown in Eq. 4,

$$\frac{t}{q_t} = \frac{1}{k_2 q_e^2} + \frac{1}{q_e} t \quad (4)$$

where k_2 is the rate constant (min^{-1}).

According to the experiment data, the relationship between t/q_e and t at different times is shown in Fig. 7b. The rate constant and adsorption capacity were calculated using the slope ($1/q_e$) and intercept ($1/k_2q_e^2$) of the line.

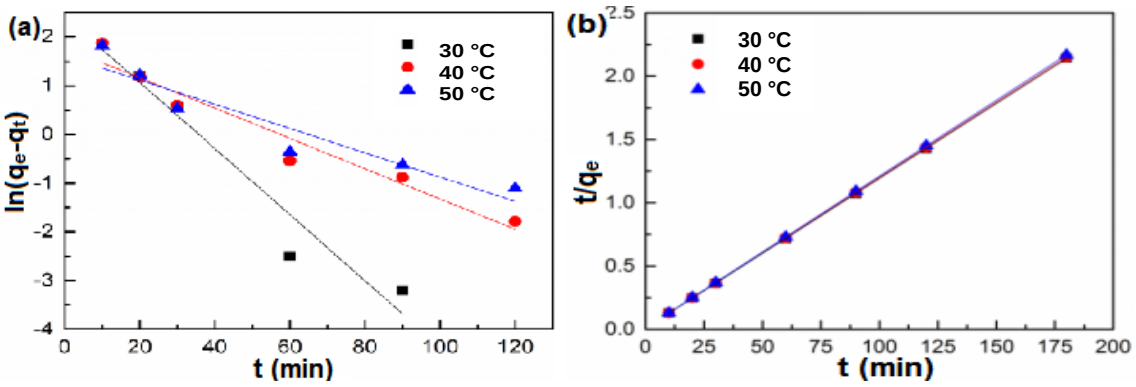

Fig. 7. Adsorption kinetics of adsorption reaction

Table 1. Related Parameters of the Adsorption Kinetics

	Pseudo-First-Order			Pseudo-Second-Order		
θ °C	k_1 (min^{-1})	q_e (mg/g)	R^2	$k_2 \times 10^{-2}$(min^{-1})	q_e (mg/g)	R^2
30	0.0311	5.9352	0.9494	1.619	84.7458	1.0000
40	1.402	11.2639	0.9510	1.402	84.0336	1.0000
50	0.3050	5.0048	0.9021	1.398	83.3333	1.0000

The adsorption kinetics parameters are shown in Table 1. There was a linear relationship between $\ln(q_e\text{-}q_t)$ and t (as shown in Fig. 7a and Fig. 7b). The reaction rate was approximately linear with the concentration of LY dye.

Comparing the results of the two models, the pseudo-second-order kinetic model better described the adsorption process. The linear fit of the experimental data presented a more linear form with R^2 equal to 1. The theoretical adsorption capacity was closer to the actual adsorption capacity. Such fits of data to the pseudo-second-order kinetic model support diffusion as the rate-determining step (Hubbe *et al.* 2019).

Adsorption Isotherm

An adsorption isotherm refers to the relationship between the amount of adsorbates attached on the surface of an adsorbent and that in the solution at adsorption equilibrium. It can describe the adsorption process and make it possible to infer the interaction between adsorbents and adsorbents.

Langmuir isotherm

The expression of the Langmuir isotherm is shown in Eq. 5,

$$\frac{Ce}{q_e} = \frac{1}{K_L q_m} + \frac{1}{q_m} Ce \quad (5)$$

where C_e is the solution concentration at equilibrium (mg/L), q_e is the adsorption capacity at equilibrium (mg/g), q_m is the maximum monolayer adsorption capacity (mg/g), and K_L is the Langmuir adsorption constant related to binding (L/mg) (Langmuir 1916).

The relationship between C_e/q_e and C_e at different adsorbent dosages is shown in Fig. 8a. The q_e, K_L, and q_m were calculated using the slope and intercept of the fit line of the Langmuir isotherm equation. The linear fit of the experimental data showed a linear form, and R^2 was close to 1.0.

Freundlich isotherm

This isotherm, based on an empirical equation, makes it possible to assume that the adsorption occurs on a heterogeneous surface at nonidentical sites with different energies of adsorption that are not always available (Freundlich 1906).

$$ln\, q\, e = ln\, K\, f + \frac{1}{n} ln\, C\, e \quad (6)$$

In Eq. 6, K_f (L/g) and n are the Freundlich constants relative to the adsorption capacity and intensity of adsorption.

According to the experimental data, the relationship between $\ln q_e$ and $\ln C_e$ at different CSCF dosages was found. The fit line of the Freundlich isotherm equation is shown in Fig. 8b. The K_f and n values were calculated using the slope and intercept of the line, and the parameter data were calculated (Table 2).

Figure 8b shows there was no linear relationship between the $\log q_e$ and $\log C_e$ of the Freundlich isothermal adsorption model. There was a good linear relationship between the C_e/q_e and C_e. The maximum of R_2 was greater than 0.95. The theoretical adsorption capacity was close to the actual adsorption capacity.

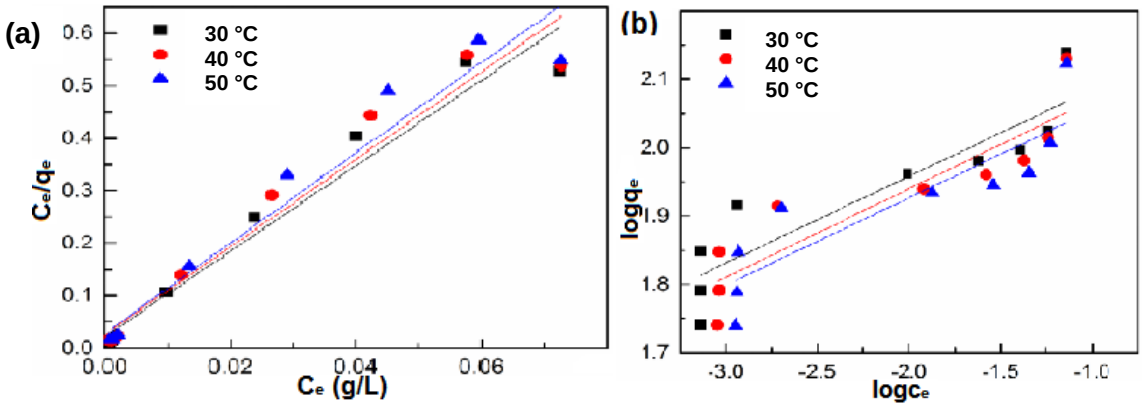

Fig. 8. Isothermal equation fitting

Table 2. Related Parameters of the Isotherms

	Langmuir			Freundlich		
θ °C	K_L (L/mg)	Q_m (mg/g)	R^2	K_f (L/g)	n	R^2
30	1.1670	104.500	0.9980	9.1349	7.8740	0.8285
40	0.3182	119.964	0.9572	9.0151	7.7220	0.8190
50	0.3050	116.260	0.9524	8.8640	7.8370	0.7808

Thermodynamic Model

In order to test the adsorption capacity of the CSCF adsorbent for LY dye, the thermodynamic parameters were introduced, *i.e.*, ΔG^0, ΔH^0, and ΔS^0. They were studied using the experimental data detailing the effects of the temperature.

The expression of the change of Gibbs free energy ΔG^0 (kJ/mol), the enthalpy change ΔH^0 (kJ/mol), and entropy change ΔS^0 (J/mol) are shown in Eqs. 7, 8, and 9, respectively,

$$K_d = \frac{q_e}{c_e} \quad (7)$$

$$\Delta G^0 = -RT\ln(K_d) \quad (8)$$

$$\ln(K_d) = \Delta S^0/R - \Delta H^0/RT \quad (9)$$

where K_d is the distribution coefficient, q_e is the adsorption capacity at equilibrium (mg/g), C_e is the solution concentration at equilibrium (mg/L), and R is the gas constant (J/mol·K) (Chen *et al.* 2019).

The experimental data of the different desorption times were put into Eq. 8 to obtain the ΔG^0. The relation line of $\ln K_d$ ~$1/T$ was plotted as shown in Fig. 9. Based on the slope and intercept of the line, ΔH^0 and ΔS^0 were calculated.

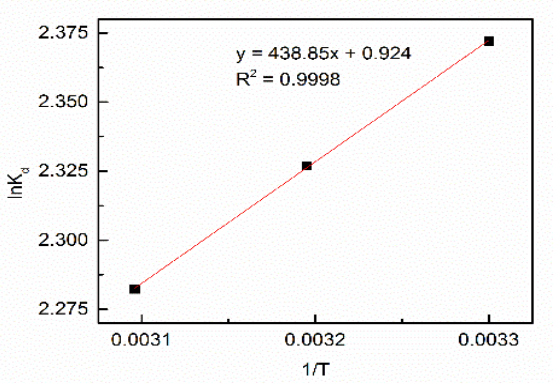

Fig. 9. The relation of lnKd ~1/*T*

Table 3. Thermodynamic Parameters

ΔH^0 (kJ/mol)	ΔS^0 (J/mol)	ΔG^0 (kJ/mol)		
		30 °C	40 °C	50 °C
-3.6486	7.6821	-5.9754	-6.0553	-6.1290

The ΔG^0 was negative in the adsorption process (as shown in Table 3), which implies that the adsorption reaction was spontaneous. The ΔH^0 was less than 0, so the adsorption process was an exothermic reaction. An increase in temperature would be unfavorable to the adsorption process.

The Analysis of Dynamic Adsorption

This analysis assumes that the probability of the decreasing adsorption rate is proportional to the probability of the adsorbate adsorption and adsorbent penetration.

The Yoon-Nelson model is simpler than other dynamic models. It does not need detailed data on the properties of the adsorbents, *e.g.*, the adsorbent, adsorbate, and fixed bed properties, so, the calculation process is simplified. This model is shown in Eqs. 10 and 11,

$$\frac{C_e}{C_o} = \frac{1}{1+\exp[k(\tau - t)]} \quad (10)$$

$$\ln \frac{C_e}{C_o - C_e} = kt - k\tau \quad (11)$$

where τ is the time taken for 50% of the adsorbate to be adsorbed (min), k is the rate constant (min^{-1}), C_o is the initial concentration of the adsorbate (mg/L), and C_e is the outflow concentration of the adsorbate (mg/L).

A line can be obtained by plotting t in terms of $\ln(C_e/(C_o - C_e))$. Using the slope and intercept of the line, k and τ were calculated.

The linear form of Yoon-Nelson model is shown as Eqs. 12 and 13,

$$t = \tau + \frac{1}{k} \ln \frac{C_e}{C_o - C_e} \quad (12)$$

$$q_o = \frac{1}{2} C_o \theta (2\tau)/m = C_o \theta \tau / m \quad (13)$$

where q_o is the mass of the adsorbate adsorbed per unit mass of adsorbent at a given flow rate (mg/g), m is the mass of the adsorbent in the column (g), and θ is the effluent rate of the adsorbent (L/min) (Enniya *et al.* 2018).

Table 4. Yoon-Nelson Model Parameters

C_o (mg/L)	$k \times 10^3$ (1/min)	q_o (mg/g)	T(min)	R^2
45.33	0.01	28.761	421	0.9536
51.53	0.02	13.157	360	0.9385

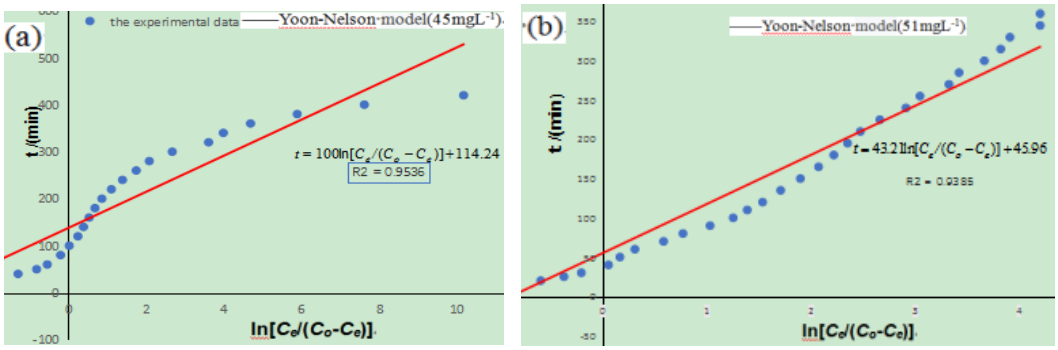

Fig. 10. Yoon-Nelson model

The Yoon-Nelson model dynamic adsorption parameters of the CSCF adsorbent for LY dye are shown in Table 4. When the concentration of the LY dye solution was 45 mg/L, the calculated theoretical data was a good fit with the experimental data (as shown in Fig. 10). The adsorption rate constants k were 0.01×10^{-3} min^{-1} and 0.02×10^{-3} min^{-1}. In a practical application, the Yoon-Nelson model is simpler than the other models because it does not consider the flow rate of the adsorbate and the adsorbent dosage. In addition, it can also obtain the time required to adsorb 50% of the adsorbent, so the adsorption efficiency can be compared.

When the initial concentration was 45 mg/L, the contact time and the effluent concentration became larger until an equilibrium was reached. In the early stage of adsorption, when the LY dye passed through the stationary phase, the CSCF had enough adsorption sites to fully absorb the dye molecules, so the effluent concentration in the initial stage was relatively low. However, with the passage of the dye solution, the CSCF adsorbs dye molecules, the adsorption sites gradually decreased, and the adsorption gradually reached saturation. Finally, the stationary phase did not have the ability to adsorb, *i.e.*, the effluent concentration was equal to the initial concentration of dye and reached equilibrium. The equilibrium time of the dynamic adsorption was 420 min.

Analysis of the Desorption and Secondary Adsorption

With the increase in desorption time, the desorption rate increased from 5 min to 35 min (as shown in Fig. 11a). After 35 min, the desorption reaction reached equilibrium and the highest desorption rate reached 98.183%. Therefore, a NaOH solution has a good desorption effect on the CSCF adsorbent after saturated adsorption of LY dye.

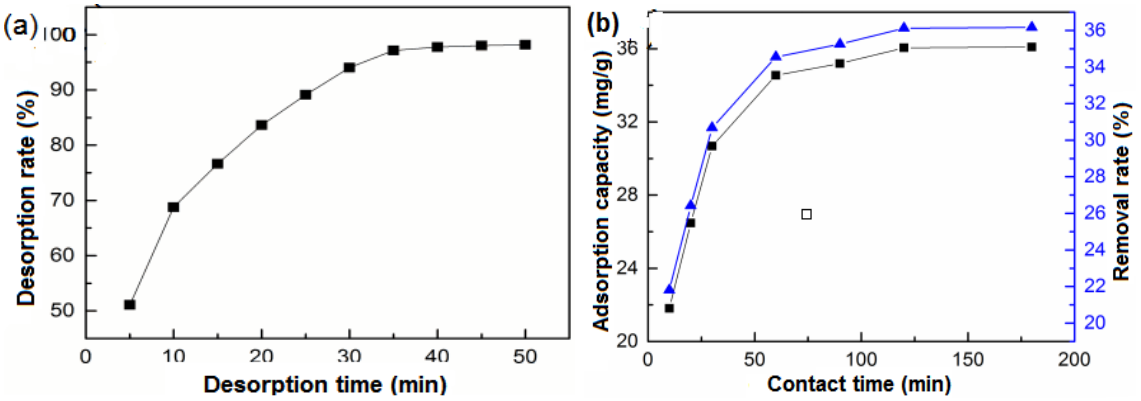

Fig. 11. The desorption and secondary adsorption

When the time was between 10 min and 120 min, when the contact time increased, the adsorption capacity and removal rate increased (Fig. 11b). At 120 min, the adsorption reaction gradually reached equilibrium. The highest adsorption capacity was 36.1 mg/g, and the highest removal rate was 36.2%. According to the experimental data, the CSCF after undergoing saturated adsorption for LY dye had a maximum adsorption capacity of 37.7 mg/g and a maximum removal percentage of 37.7%. The experimental results shows that the adsorption capacity and removal extent of the CSCF secondary adsorption after the desorption were similar to those of the first adsorption. Therefore, the saturated CSCF adsorbent for LY dye still showed good adsorption performance after undergoing desorption.

CONCLUSIONS

1. A cationic straw cellulose fiber (CSCF) adsorbent was prepared *via* cationic modification with SCF. The optimal adsorption conditions of the CSCF for light yellow (LY) dye were as follows: a pH of 4, a temperature of 30 °C, a CSCF dosage of 0.4 g/L, an initial concentration of 50 mg/L, and a contact time between the CSCF and LY dye of 90 min.
2. Results showed that the highest adsorption capacity was 137.6 mg/g and the highest removal percentage was 99.3%. The pseudo-second-order kinetic model described the adsorption process well, and it also conformed to the Langmuir isotherm model. The thermodynamic model described that the adsorption reaction was spontaneous, and the adsorption process was an exothermic reaction.
3. Dynamic adsorption testing showed that the time to reach equilibrium was 420 min when the concentration of the LY dye solution was 45 mg/L. The theoretical data calculated using the Yoon-Nelson model had a good fit with the experimental data. After desorption *via* a diluted NaOH solution, the maximum adsorption capacity was still 36.1 mg/g and the maximum removal rate still reached 36.2%.
4. This work showed that CSCF was an efficient biosorbent for dye wastewater purification process. Its preparation and use provide a new method for the effective utilization of rice straw resources.

ACKNOWLEDGMENTS

The authors are grateful for the support of the Fundamental Research Funds for the Central Universities, Grant No. 2572017CB08.

REFERENCES CITED

Alver, E., Bulut, M., Bulut, M., Metin A. U., and Ciftci, H. (2017). "One step effective removal of Congo Red in chitosan nanoparticles by encapsulation," *Spectrochimica Acta Part A: Molecular and Biomolecular Spectroscopy* 171(1), 132-138. DOI: 10.1016/j.saa.2016.07.046

Asfaram, A., Ghaedi, M., Hajati, S., Goudarzi, A., and Dil, E. A. (2017). "Screening and optimization of highly effective ultrasound-assisted simultaneous adsorption of cationic dyes onto Mn-doped Fe_3O_4-nanoparticle-loaded activated carbon," *Ultrasonics Sonochemistry* 34(1), 1-12. DOI: 10.1016/j.ultsonch.2016.05.01

Baldikova, E., Safarikova, M., and Safarik, I. (2015). "Organic dyes removal using magnetically modified rye straw," *Journal of Magnetism and Magnetic Materials* 380(4), 181-185. DOI: 10.1016/j.jmmm.2014.09.003

Chen, K., Zhang, Z., Xia, K., Zhou, X., Guo, Y., and Huang, T. (2019). "Facile synthesis of thiol-functionalized magnetic activated carbon and application for the removal of mercury(II) from aqueous solution," *ACS Omega* 4(5), 8568-8579. DOI: 10.1021/acsomega.9b00572

Ciftci, D., Flores, R. A., and Saldaña, M. D. A. (2018). "Cellulose fiber isolation and characterization from sweet blue lupin hull and canola straw," *Journal of Polymers and the Environment* 26(7), 2773-2781. DOI: 10.1007/s10924-017-1164-5

De, D., Santosha, S., Aniya, V., Sreeramoju, A., and Satyavathi, B. (2018). "Assessing the applicability of an agro-industrial waste to engineered bio-char as a dynamic adsorbent for Fluoride Sorption," *Journal of Environmental Chemical Engineering* 6(2), 2998-3009. DOI: 10.1016/j.jece.2018.04.021

Elumalai, S., Agarwal, B., Runge, T. M., and Sangwan, R.S. (2016). "Integrated two-stage chemically processing of rice straw cellulose to butyl levulinate," *Carbohydrate Polymers* 150(10), 286-298. DOI: 10.1016/j.carbpol.2016.04.122

Enniya, I., Rghioui, L., and Jourani. A. (2018). "Adsorption of hexavalent chromium in aqueous solution on activated carbon prepared from apple peels," *Sustainable Chemistry and Pharmacy* 7(3), 9-16. DOI: 10.1016/j.scp.2017.11.003

Fan, S., Wang, Y., Wang Z., Tang, J., and Li., X. (2017). "Removal of methylene blue from aqueous solution by sewage sludge-derived biochar: Adsorption kinetics, equilibrium, thermodynamics and mechanism," *Journal of Environmental Chemical Engineering* 5(1), 601-611. DOI: 10.1016/j.jece.2016.12.019

Freundlich, H. M. F. (1906). "Over the adsorption in solution," *Journal of Physical Chemistry* 57, 4574-4578.

Ge, Y., Wang, C., Liu, S., and Huang, Z. (2016). "Synthesis of citric acid functionalized magnetic graphene oxide coated corn straw for methylene blue adsorption," *Bioresource Technology* 221(12), 419-429. DOI: 10.1016/j.biortech.2016.09.060

Ghasemi, S. M., Ghaderpoori, M., Moradi, M., Taghavi, M., and Karimyan, K. (2020). "Application of Box-Behnken design for optimization of malachite green removal

from aqueous solutions by modified barley straw," *Global NEST Journal* 22(3), 390-399. DOI: 10.30955/gni.003089

Halysh, V., Sevastyanova, O., Pikus, S., Dobele, G., Pasalskiy, B., Gun'ko, V. M., and Kartel, M. (2020). "Sugarcane bagasse and straw as low-cost lignocellulosic sorbents for the removal of dyes and metal ions from water," *Cellulose* 27(14), 8181-8197. DOI: 10.1007/s10570-020-03339-8

Heibati, B., Rodriguez-Couto, S., Al-Ghouti, M. A., Asif, M., Tyagi, I., Agarwal, S., and Gupta, V. K. (2015). "Kinetics and thermodynamics of enhanced adsorption of the dye AR 18 using activated carbons prepared from walnut and poplar woods," *Journal of Molecular Liquids* 208(9), 99-105. DOI: 10.1016/j.molliq.2015.03.057

Hosseini, S. A., Vossoughi, M., Mahmoodi, N. M., and Sadrzadeh M. (2018). "Efficient dye removal from aqueous solution by high-performance electrospun nanofibrous membranes through incorporation of SiO_2 nanoparticles," *Journal of Cleaner Production* 183(5), 1197-1206. DOI: 10.1016/j.jclepro.2018.02.168

Hu, D., and Wang, L. (2016). "Adsorption of ciprofloxacin from aqueous solutions onto cationic and anionic flax noil cellulose," *Desalination and Water Treatment* 57(58), 28436-28449. DOI: 10.1080/19443994.2016.1183232

Hu, L., Zang, L., Liu Q., Qiu, J., Yang, C., Xu, X., Yang, J., and Qiao, X. (2019). "Effective and selective removal of cationic dye from aqueous solution using rosin derivative modified wheat straw," *Desalination and Water Treatment* 153(6), 349-356. DOI: 10.5004/dwt.2019.24006

Hubbe, M. A., Azizian, S., and Douven, S. (2019). **"**Implications of apparent pseudo-second-order adsorption kinetics onto cellulosic materials. A review," *BioResources* 14(3), 7582-7626. DOI: 10.15376/biores.14.3.7582-7626

Langmuir, I. (1916). "The constitution and fundamental properties of solids and liquids: Part I. Solids," *Journal of the American Chemical Society* 38(11), 2221-2295. DOI: 10.1021/ja02268a002

Li, X., and Li, Y. (2019). "Adsorptive removal of dyes from aqueous solution by $KMnO_4$-modified rice husk and rice straw," *Journal of Chemistry* 2019(8), 1-9. DOI: 10.1155/2019/8359491

Lima, D. R., Sellaoui L., Klein, L., Reis, G. S., Lima, É. C., and Dotto, G. L. (2018). "Physicochemical and thermodynamic study of malachite green adsorption on raw and modified corn straw," *Canadian Journal of Chemical Engineering* 96(3), 779-787. DOI: 10.1002/cjce.22948

Patil, P. R., Marathe, Y. V., and Shrivastava, V. S. (2015). "Evaluation of the adsorption kinetics and equilibrium for the potential removal of Congo red dye from aqueous medium by using a biosorbent," *British Journal of Applied Science & Technology* 6(6), 557-573. DOI: 10.9734/BJAST/2015/12590

Sudhan, N., Subramani, K., Karnan, M., IIayaraja, N., and Sathish, M. (2016). "Biomass-derived activated porous carbon from rice straw for high energy symmetric supercapacitor in aqueous and non-aqueous electrolytes," *Energy & Fuels* 31(1), 977-985. DOI: 10.1021/acs.energyfuels.6b01829

Sun, Y., Wu Z.-Y., Wang, X., Ding, C., Cheng, C., Yu, S.-H., and Wang, X. (2016). "Macroscopic and microscopic investigation of U(VI) and Eu(III) adsorption on bacterium-derived carbon nanofibers," *Environmental Science & Technology* 53(19), 4459-4467. DOI: 10.1021/acs.est.9b04434

Xia T., Wang Y., and Fan, P. (2013). "Study on adsorption of modified rice hull for methylene blue simulated wastewater," *Industrial Water Treatment* 33(3), 47-50.

Xie, M., Xiong F. P., Feng, C. L., Han, J. J. and Wu, X. (2019). "Preparation of cellulose-graphene oxide composite and its adsorption for Pb^{2+}," *Technology of Water Treatment* 45(8), 67-70.

Zazycki, M. A., Godinho, M., Perondi, D., Foletto, E. L., Collazzo, G. C., and Dotto, G. L. (2017). "New biochar from pecan nutshells as an alternative adsorbent for removing reactive red 141 from aqueous solutions," *Journal of Cleaner Production* 171(1), 57-65. DOI: 10.1016/j.jclepro.2017.10.007

Zhang, X., Jin, C., Jiang, Y., Liu, G., Wu, G., and Kong, Z. W. (2017). "A novel gallic acid-grafted-lignin biosorbent for the selective removal of lead ions from aqueous solutions," *BioResources* 12(3), 5343-5357. DOI: 10.15376/biores.12.3.5343-5357

Zhu, L., Shen, F., Smith, R. L., Yan, L., Li, L., and Qi, X. (2017). "Black liquor-derived porous carbons from rice straw for high-performance supercapacitors," *Chemical Engineering Journal* 316(5), 770-777. DOI: 10.1016/j.cej.2017.02.034

Article submitted: February 21, 2021; Peer review completed: March 28, 2021; Revised version received and accepted: April 7, 2021; Published: April 20, 2021.
DOI: 10.15376/biores.16.2.3991-4006